Erez Hasman
e-mail: mehasman@technion.ac.il

Vladimir Kleiner

Nir Dahan

Yuri Gorodetski

Kobi Frischwasser

Igal Balin

Micro and Nanooptics Laboratory,
Faculty of Mechanical Engineering,
Russell Berrie Nanotechnology Institute,
Technion-Israel Institute of Technology,
Haifa 32000, Israel

Manipulation of Thermal Emission by Use of Micro and Nanoscale Structures

In high temperature and vacuum applications, for which heat transfer is predominantly by radiation, the material's surface texture is of substantial importance. Several micro and nanostructures designs have been proposed to enhance a material's emissivity and its radiative coherence. Control of thermal emission is of crucial concern in the design of infrared sources, in electronic chip coolants, in high-efficiency photovoltaic cells, and in solar energy conversion. In this review paper, we present microscale and nanoscale structures supporting surface waves for obtaining polarization manipulation of thermal emission, extraordinary coherent thermal radiation, bandgap in the spectral emission, spin symmetry breaking of coupled thermal antenna array, and a broadband infrared absorption. [DOI: 10.1115/1.4005160]

Keywords: coherence, thermal emission, surface waves, coupled cavities, bandgap, metamaterials, polarization, spin-orbit interaction

1 Introduction

Thermal emission of absorbing materials is affected by surface morphology as well as the excitation of surface waves: surface plasmon-polaritons in metal or surface phonon-polaritons in polar crystal. Surface waves are confined electromagnetic waves due to collective oscillations of the free electrons in metal or the resonant collective lattice vibrations in polar crystal, which propagate along the interface and decay exponentially with increasing the distance from the interface. The electromagnetic energy density associated with surface waves has been widely investigated. It has been shown that thermal emission can be quasi-monochromatic in the vicinity of a flat surface, in a distance that is of the order of a wavelength, due to the excitation of resonant surface waves. Furthermore, surface modes yield a long-range spatial coherence length, on a scale of the surface wave propagation length, which may be much larger than the emitted wavelength. To transmit these surface waves along with their coherency to the far-field, several configurations were suggested, such as, gratings, multilayer structure, photonic crystals, and resonant cavities.

In the first section of this article, space-variant polarization manipulation of enhanced omnidirectional thermal emission in a narrow spectral peak is presented. The emission is attributed to surface phonon-polariton (SPhP) excitation from space-variant subwavelength SiO_2 gratings. Polarization manipulation was obtained by discretely controlling the local orientation of the grating. We experimentally demonstrated thermal emission in an axially symmetric polarization distribution. Theoretical calculations based on rigorous coupled-wave analysis are presented along with experimental results.

In the second section, the enhanced coherency is discussed which is due to coherent coupling between resonant cavities (thermal micro-antennas) obtained by surface standing waves, wherein each cavity supports a localized field that is attributed to coupled SPhPs. We demonstrate an extraordinary coherent thermal radiation from coupled resonant cavities. The coupling is implemented by surface standing waves between the cavities. As a result, the spatial coherence length is increased by an order of magnitude compared with that of delocalized surface waves.

In Sec. 3, we present an experimental observation of wide bandgap of thermally excited SPhP. Formation of the bandgap and coupling SPhP to radiative waves is done by a binary biharmonic structure formed on a SiC substrate. Such a structure modifies the dynamic of the surface wave and results in a characteristic Van Hove singularity in the spectral density of states (DOS) of the SPhPs.

Moreover, in Sec. 4, we introduce manipulation of a thermal radiation by use of inhomogeneous and anisotropic structures which results in several symmetry breaking effects. Geometric Doppler effect manifested by a spin-split dispersion relation of thermal radiation is observed. A spin-dependent dispersion splitting was obtained in a structure consisting of a coupled thermal antenna array. The effect is due to a spin-orbit interaction resulting from the dynamics of the surface waves propagating along the structure whose local anisotropy axis is rotated in space. The observation of the spin symmetry breaking in thermal radiation may be utilized for manipulation of spontaneous or stimulated emission.

Section 5 is devoted to metallic subwavelength structures for a broadband thermal infrared absorption control. Highly absorbing thin metallic films are widely used in applications such as thermal microbolometric and pyroelectric cameras. We present a method to control the absorption of a thin film resonator by using a subwavelength structure consisting of metallic plates that behaves as a metamaterial film.

2 Space-Variant Polarization Manipulation of Thermal Emission by Subwavelength Grating Supporting Surface Phonon-Polaritons

Spontaneous emission from absorbing material is considered to be incoherent and unpolarized. The surface properties of the absorbing material have a profound impact on the emission's optical properties, and can be manipulated to produce a partially coherent and partially polarized radiation [1–4]. A connection between the emission and the surface properties was established by studying the excitation of SPhPs [1]. Surface polariton has a longer wave vector than the light waves propagating along the surface with the same frequency. For this reason, they are called "nonradiative" surface polaritons. By coupling the surface polaritons with the propagating wave by means of an additional prism

Contributed by the Heat Transfer Division of ASME for publication in the JOURNAL OF HEAT TRANSFER. Manuscript received November 3, 2010; final manuscript received January 20, 2011; published online January 20, 2012. Assoc. Editor: Jungho Kim.

or grating, one can produce either increased resonant absorption or emission. Because SPhPs are able to be excited only by transverse magnetic (TM) polarized propagating waves, the emission's characteristics have to be polarization dependent.

We introduce a theoretical and experimental investigation of space-variant polarization-dependent thermal emission by exploiting the polarization dependence of the SPhPs [5,6]. Subwavelength gratings etched on fused silica (SiO_2) substrates are used to generate space-variant polarization radiation. As a first step, we designed a grating to enhance the omnidirectional thermal emission to form a narrow spectral peak for TM polarization. We experimentally demonstrated space-variant polarization manipulation of thermal emission by discretely controlling the local orientation of the grating. This phenomenon can be exploited in a variety of applications such as thermal polarization imaging, spatially modulated heat transfer, and the formation of high-efficiency thermal sources.

Polar materials support SPhPs in the spectral range where $\varepsilon' < -1$ (ε' is the real part of the dielectric constant). Fused silica behaves as a polar material in the range of 8.65 μm–9.18 μm. In order to maximize the emissivity, we optimized the SiO_2 grating using a spectral reflectance numerical calculation by rigorous coupled-wave analysis (RCWA) method. Let us define the relative emissivity as the grating emissivity (ε_G) normalized to the emissivity of the flat surface (ε_F). A narrow spectral peak of $\Delta\lambda = 90$ nm was obtained from a grating with period 2 μm, fill factor $q = 0.3$, and grating depth $h = 0.8$ μm for TM polarization around a wavelength of 9.07 μm, as seen in Fig. 1(*a*). Figure 1(*b*) indicates that the peak is nondirectional. Its relative emissivity was 2.75, while the relative emissivity of transverse electric (TE) polarization was approximately unity. In order to demonstrate space-variant polarization-dependent thermal emission, we formed space-variant spiral elements having a discrete local groove orientation [5–8], see Fig. 1(*c*). The emitted radiation was passed through polarizer. Space-variant propeller-shaped intensity modulation, resulting from the space-variant polarization-dependent emissivity, is clearly observed in Fig. 1(*d*). The distribution of the emissions from the spiral elements not passed through a polarizer are shown in Fig. 1(*e*). In this case, the emission distribution is almost uniform. However, an axially symmetric polarization orientation is obtained in the near field for the enhanced TM emission.

In conclusion, using the polarization dependence of the emissivity, a space-variant polarization manipulation of the thermal emission was experimentally demonstrated by controlling the local orientation of the subwavelength grating.

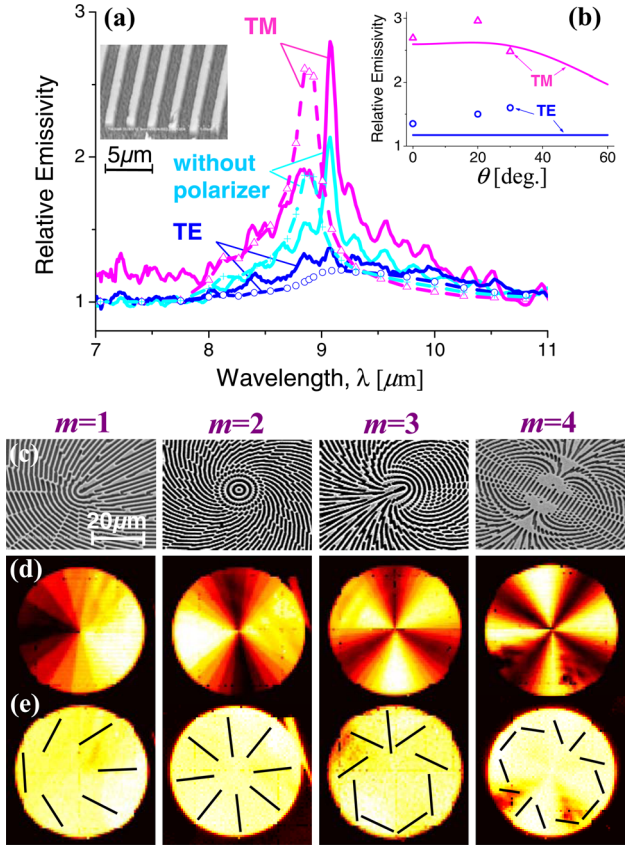

Fig. 1 (*a*) Measured (solid) and calculated (dashed) relative emissivity spectrum of the grating for TM, TE polarization, and without a polarizer in normal observation direction, with grating parameters: period 2 μm, fill factor 0.3, and depth 0.8 μm. The element was heated to a temperature of 873 K. The inset shows a scanning electron microscope (SEM) image of the grating. (*b*) Measured and calculated (solid) relative emissivity as a function of observation angle. (*c*) SEM images of the spiral subwavelength elements with polarization order numbers $m = 1$, 2, 3, and 4. (*d*) Thermal emission images emerging from the SiO_2 spiral elements captured through a polarizer and (*e*) without a polarizer. The lines indicate the local TM polarization orientation measured in the near field. The elements were uniformly heated to a temperature of 353 K.

3 Extraordinary Coherent Thermal Emission of Coupled Resonant Cavities due to Surface Waves Excitation

Surface waves have been shown to play a key role in spontaneous thermal emission in the near field, and dramatically affect the local DOS in the vicinity of an interface, as well as the coherence properties of the nonradiative field [9–15]. The near field coherence of the delocalized nonradiative surface waves can be transferred into radiative fields by introducing shallow grating on the surface [1,5]. However, such a grating only causes a smooth perturbation to the surface; therefore, the emission pattern had a rainbow-like behavior, and the coherence length in the far-field was found to be limited by that of the delocalized surface waves.

We investigate theoretically and experimentally an extraordinary coherent thermal radiation of coupled resonant cavity (CRC) structure [16,17] etched on a SiC substrate, see Fig. 2(*a*). We show that it is possible to obtain a quasi-monochromatic thermal source with a high quality factor $Q \approx 600$, which corresponds to highly temporal coherence, and a spatial coherence length 716λ ($\lambda = 11.6$ μm) associated with extraordinary directivity, see Figs. 2(*b*)–2(*d*). The source supports a thermal emission at a single resonant frequency and in a well-defined direction, as opposed to coupling delocalized SPhPs using a shallow grating. This resonant enhancement could be obtained for TM polarized wave due to CRC structure in the spectral range where SiC supports SPhPs. The CRC structure consists of periodic cavities in which each cavity supports standing waves, and the adjacent cavities are coupled by surface standing waves. The magnitude of the electric field was calculated by a finite difference time domain (FDTD) algorithm as shown in Figs. 2(*e*) and 2(*f*). Standing waves are clearly discerned inside the cavities where each isolated cavity can be regarded as a localized source supporting a broad angular emission. In order to obtain a directional emission, a coherent coupling mechanism between the cavities is required. By choosing the periodicity of the cavities according to Rayleigh's anomaly, a surface standing wave is excited, which correlates adjacent resonant cavities, see Fig. 2(*f*). As a result, we obtained a resonant frequency having a coherency for a longer distance than that of the delocalized SPhPs [1], yielding a highly directional emission.

In conclusion, by utilizing periodic coupled resonant cavities, a very high coherent thermal source can be designed, which is not limited by the coherence of the delocalized surface waves. Controlling the emission (or absorption) behavior of a system is a substantial role in radiative energy transfer and energy conversion. Furthermore, the high resonance structure may be implemented in

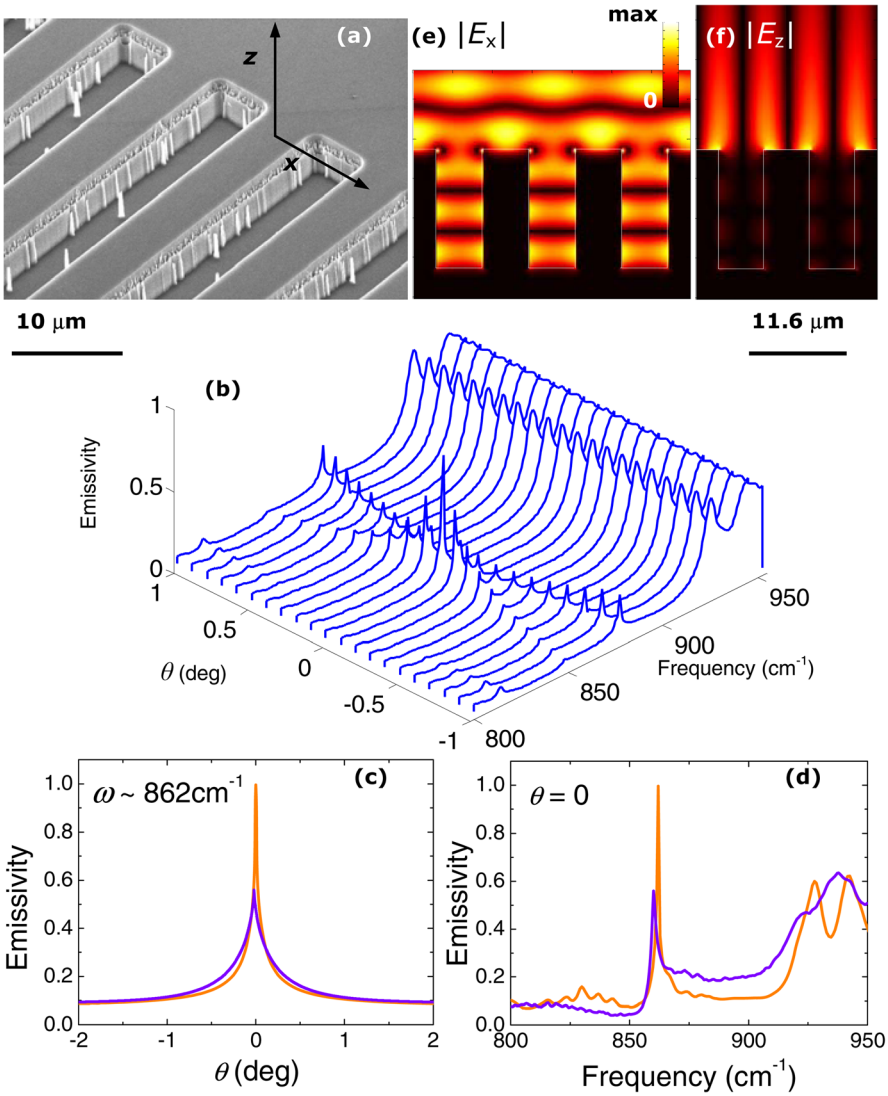

Fig. 2 (*a*) SEM image of CRC structure upon SiC, with period of 11.6 μm, fill factor 0.56, and cavity depth of 4.6 μm. (*b*) Theoretical emissivity distribution as a function of frequency and observation angle θ. (*c*) Calculated (orange) and experimental (purple) directional emissivity at the peak frequency and (*d*) spectral emissivity in the normal direction. (e) Calculated electric field distribution in the *x-z* plane, $|E_x|$ and (f) $|E_z|$.

absorption mechanism, by use of surface plasmons in the visible spectra to attain higher sensitivity sensing devices.

4 Bandgap Structure of Thermally Excited Surface Phonon-Polaritons

Conventional thermal sources usually have a broad spectrum and isotropic emittance. However, recent works have shown that coherent thermal emission can be obtained by electromagnetic surface waves excitation [1,17–20]. The emission properties, such as coherence length or energy density, can be engineered by modifying the dynamics of the surface waves, for instance, by localization. One of the ways to achieve this localization is by introducing a Bragg grating on the surface of the polaritonic material which results in a bandgap in the dispersion curve [21]. At the bandgap's edges, the density of the surface modes has a Van Hove singularity [22], thus, the field is strongly enhanced near the air-substrate interface. This can be exploited to enhance second harmonic generation [23], Raman scattering [24], photoluminescence [25], fluorescence [26], and absorption. A convenient method of observing these energy gaps is by coupling the polaritons to propagating waves. For this purpose, an additional grating component is essential [21]. By composing the Bragg and the coupler components a binary biharmonic structure (BBS) is created such that the radiative waves carry information about the bandgap. In many cases, a large gap width is required. For example, when introducing a defect inside the Bragg grating, localization of modes with frequencies inside the bandgap is allowed [27,28]. As the gap width increases, the localized modes are resolved more clearly. It was shown that the plasmonic gap width ($\delta\omega$) depends on the real part of the complex permittivity of metal, $\delta\omega \propto 1/\sqrt{|\varepsilon'|}$. Since surface waves are excited in the spectral region where $\varepsilon'(\omega) < -1$, the largest gap width is expected to be found near the resonance frequency, corresponding to $\varepsilon'(\omega) \sim -1$. According to Wien's law, thermal emission has its maximum value in the mid-infrared (mid-IR) region at room temperature. Since the resonance frequency in metals is usually located in the *ultraviolet/visible* spectra range, only a small bandgap was observed in the mid-IR region [28]. In order to achieve a large bandgap, it is reasonable to use polar materials such as SiC or SiO_2 which have resonance frequencies in the mid-IR region.

We observe a wide bandgap of thermally excited SPhPs [30]. Formation of the bandgap and coupling to the radiative waves is produced by a biharmonic structure formed on a SiC-6H

substrate. We experimentally verified that the DOS near the bandgap has a characteristic one-dimensional (1D) Van Hove singularity. In addition, an inverse relation was found between the gap width and the squared spatial coherence length of the emitted thermal radiation at the band extrema frequencies, whereas the spectral quality factor remained constant. This feature can be utilized to design thermal emitters, polaritonic bandgap microcavities for sensing applications, and thermophotovoltaic systems.

We investigate thermal emission from a binary coupler grating and BBSs with various amplitude of a Bragg to coupler harmonics ratio $R = A_2/A_1$. The samples were realized using standard photolithographic techniques on a SiC substrate, with a periodicity $\Lambda = 11.2\,\mu$m, depth $h = 510$ nm, and filling factor 0.5. A SEM image of the magnified area is shown in Fig. 3(*a*). The selected periodicity of the structures ensured coupling of the surface waves at the resonance frequency $\omega_0/2\pi c = 844$ cm^{-1} (corresponds to $\lambda_0 = 11.84\,\mu$m) to radiative waves at a normal direction. Measurements were performed using a Fourier transform infrared spectrometer, while heating the sample to 773 K. Figure 3(*c*) shows the dispersion of SPhPs measured by thermal emission from the binary coupler grating along with a calculation based on a RCWA method. The bright colors represent high emissivity. The bandgap width is proportional to the grating depth, so that in a shallow grating ($h = 300$ nm), a bandgap does not appear. The measured and the calculated emissions from the BBSs are shown in Figs. 3(*d*)–3(*f*). Wide bandgaps are observed: $\delta\omega/\omega_0 = 0.03$, 0.04, and 0.05 for $R = 2/3$, 4/5, and 1, respectively. These large gaps could be attributable in the mid-IR to the small permittivity of SiC in this spectrum. The gap width dependence on the ratio of the amplitudes, R is evident from Figs. 3(*b*) and 3(*d*)–3(*f*). As can be seen, the gap width increases as the ratio between the first two harmonics increases. Furthermore, we calculated the group velocity from our measurements (see Figs. 3(*c*)–3(*f*)) near the bandgap edge frequencies and observed that in BBSs the DOS linearly depends on $|\omega - \omega_{\pm}|^{-1/2}$, as expected from the Van Hove theorem [22] for 1D structure.

According to Kirchhoff's law, enhanced emission of a BBS corresponds to enhanced absorption. Thus, a narrow absorption spectral resonance can be obtained in a wide range of angles utilizing a wide bandgap structure. This property can be exploited to design a mid-IR refractive-index sensor based on spectral resonant excitation of SPhPs [31], which will not require a high coherence thermal source.

5 Spin Symmetry Breaking in Thermal Emission

When light is emitted or scattered from a revolving medium, it exhibits a dispersion splitting—angular Doppler effect—which depends on the circular polarization handedness (the photon's spin) [32–34]. The dispersion splitting is attributed to a spin-dependent correction of the momentum term in the wave equation due to a rotation of the emitting medium. This splitting is the manifestation of the spin-orbit interaction, which is the basis for optical spin-Hall [35,36], Magnus [37], and Coriolis effects [38,39]. Here, we report on a geometric Doppler effect manifested by a spin-dependent dispersion splitting of thermal radiation emitted from a structure whose local anisotropy is rotated along x-axis (superstructure). The observed effect is attributed to the dynamics of the thermally excited surface wave propagating along the superstructure [40].

In our experiment, a subwavelength $1.2\,\mu\text{m} \times 4.8\,\mu$m rod array with a periodicity of $\Lambda = 11.6\,\mu$m was etched to a depth of $1\,\mu$m on a SiC substrate, Fig 4(*a*). In Fig 4(*b*), we present the measured dispersion of the thermal emission from the homogeneous rod array locally oriented at an angle of 30 deg (Fig. 4(*a*)—top). The plot consists of a fast mode related to the usual delocalized surface waves, and a slow mode attributed to coupled, localized phonon-polaritons. By applying polarization measurements, we verified that the polarization direction of the slow mode follows the rods' orientation. Next, an array of rods whose orientation was gradually rotated along the x-axis was studied (Fig 4(*a*)—bottom). In the measured dispersion (see the Fig 4(*c*)) the slow mode exhibits a clear splitting in the momentum.

The above phenomenon can be elucidated when considering surface waves propagation. As SPhPs travel along the superstructure, they radiate a linearly polarized field that rotates at a spatial rate $\Omega = d\phi/dx$ (ϕ—local rod's orientation). This rotation induces coupling between the intrinsic and the extrinsic degrees of freedom—spin-orbit interaction—which leads to a spin-dependent perturbation of the momentum $\Delta k = \sigma\Omega$, where $\sigma = \pm 1$ is the spin state [36,41]. By solving the perturbated Helmholtz equation we derive the dispersion shift in the momentum dimension, $\omega = \omega(k_x + \sigma\Omega)$. Therefore, the original dispersion of the

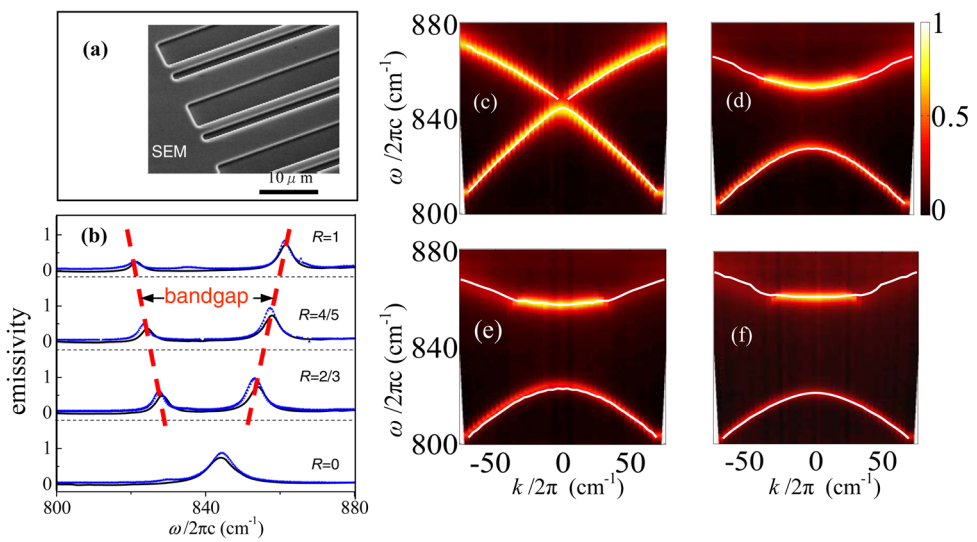

Fig. 3 (*a*) SEM image of realized BBS with period $\Lambda = 11.2\,\mu$m, depth $h = 510$ nm, and amplitude ratio $R = 1$. (*b*) Measured (blue dots) and calculated (black solid curves) spectral emissivity at normal incidence ($k = 0$). One can see the bandgaps for several values of R; dashed red lines indicate locations of the bandgaps. Measured dispersion of thermal emission from binary coupler grating (*c*), and BBSs with $R = 2/3$ (*d*), $R = 4/5$ (*e*), and $R = 1$ (*f*). RCWA calculations are depicted by solid white lines.

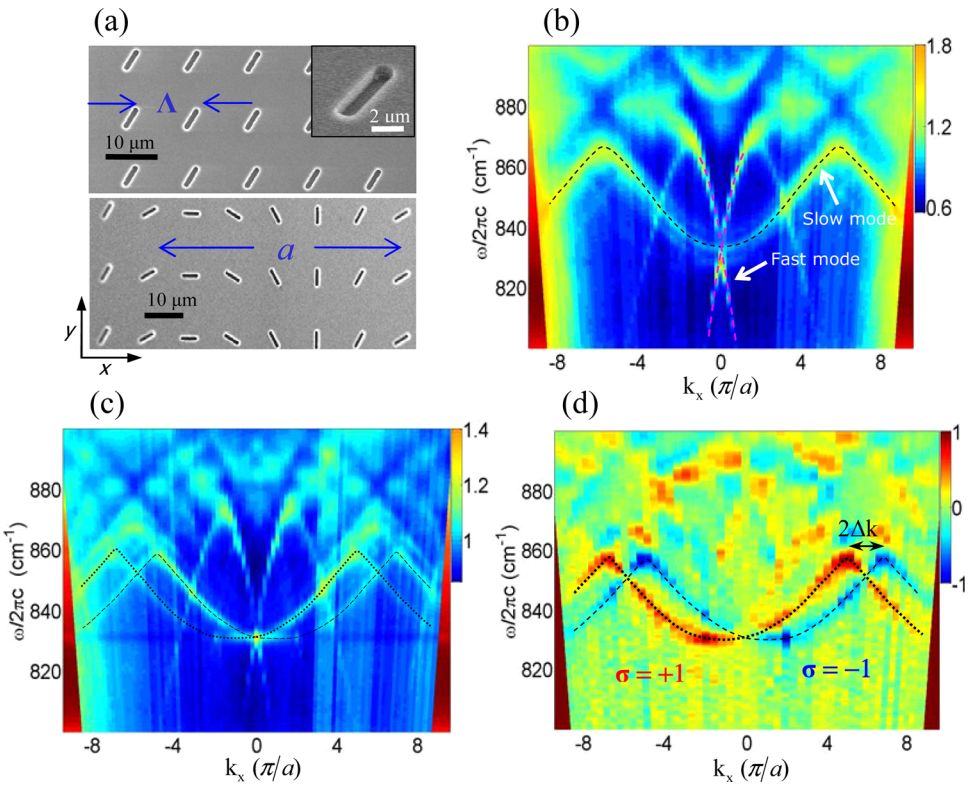

Fig. 4 (*a*) top: SEM image of the homogeneous rod array (1.2 μm × 4.8 μm, $\Lambda = 11.6$ μm, depth of 1 μm on a SiC); bottom: SEM of the rod array rotating along the x-axis with a period $a = 6\Lambda$ ($\Omega = \pi/a$); inset—SEM image of a single rod. (*b*) The measured emission dispersion of the homogeneous rod array. Dashed lines highlight the dispersion of the slow and the fast modes. (*c*) Measured dispersion of the rotating rod array. Dashed/dotted black lines indicate the split slow modes. (*d*) Spin-projected dispersion of the rotating rod array, obtained by S_3 measurement. Dashed/dotted lines highlight the dispersion of the spin-split slow mode (red/blue color corresponds to a positive/negative spin projection, respectively). The observed dispersion shift is $\Delta k = \sigma\Omega$.

homogeneous structure is split into two emitted modes with opposite spin states. To verify the proposed model, we measured the spin-projected dispersion emitted from the element by measuring the Stokes' parameter S_3, which represents the circular polarization portion. This measurement reveals that the slow mode is indeed shifted by $\Delta k = \sigma\Omega$, as predicted (see Fig 4(*d*)). Our experiment paves the way to manipulate spontaneous emission with the photons' intrinsic degree of freedom and provides the basis for future spinoptics devices [42].

6 Metallic Subwavelength Structures for a Broadband Infrared Absorption Control

The use of highly absorbing thin metallic films is crucial in applications such as microbolometric and pyroelectric cameras, and thermal detectors, which are used in the midinfrared to the microwave radiation region [43]. These cameras are mostly used in stellar imaging and in the detection of covered objects, as well as for biological imaging. When describing the structure of absorbing metallic films, several methods have been employed. The "black metal absorber" design [44–46] consists of a thin, granular metal film. The process of forming such a film is not repetitive. Another approach is based on utilizing a thin metallic film with thickness in the nanometer range in a resonator configuration. The absorption property of a thin metallic film is a function of the layer conductivity, $\sigma \propto nk$ (n, k are the refractive-index and extinction coefficient of the material), and its thickness, h [47,48]. However, fabricating a uniformly thin metallic film is not repetitive and suffers from adhesion problems. Furthermore, such a film is sensitive to thickness errors due to inhomogeneity.

We propose using a subwavelength periodic structure embedded in a metal film to control absorption in a resonator configuration, see Fig. 5(*a*) [49]. By varying the structure's parameters, e.g., period (Λ), fill factor (q), thickness and shape (S), we can tailor the conductivity of the subwavelength structure, i.e., $\sigma = \sigma(\Lambda, q, h, \mathrm{S})$ to achieve a resonator with the desired impedance matching. We demonstrated the ability to obtain an absorber that has a thickness of tens of nanometers, effectively overcoming the difficulties encountered by the thin film method. Figure 5(*b*) describes σ at 11 μm wavelength as a function of the area fill factor, q^2, of the metallic structures, for the effective medium approximation and the FDTD calculation, as well as the measured results. A close agreement between both calculations and the measured results is clearly observed. In addition, we see the expected linear dependence of σ as a function of q^2 for the subwavelength metallic plates. Figure 5(*b*) also depicts the case of subwavelength metallic spheres. This structure is approximated by the Maxwell-Garnett effective medium theory [50]. Using this structure, one can see the small dynamic range provided by structural property modification.

We calculated characteristics of the resonant absorber (see Fig. 5(*a*)) using the measured properties of the metallic structure. Figure 5(*c*) shows the absorption of the resonator as a function of the wavelength where a broadband enhanced absorption is obtained. For comparison, we present the resonator configuration for NiCr film absorber with thickness of 30 nm.

To conclude, the manipulation of the absorption is performed by controlling the structure's parameters. Such an approach is applicable for advanced microbolometric cameras for any spectral range. Furthermore, a space-variant manipulation of the absorption

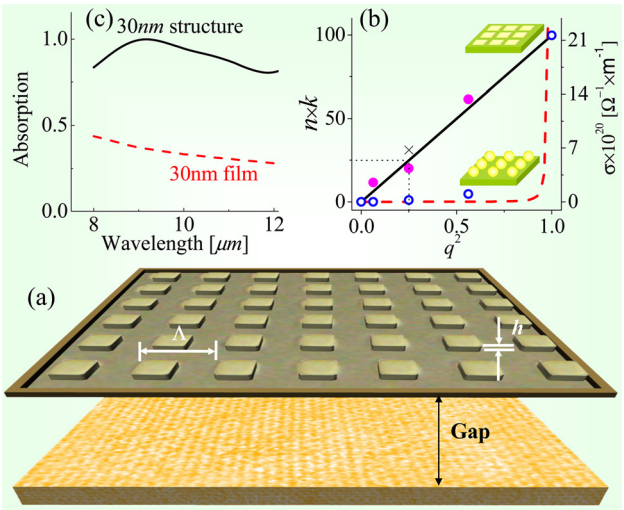

Fig. 5 (*a*) Concept of a resonant absorber using a metallic subwavelength structure as a metamaterial absorbing layer including a microscope image of the measured NiCr structure with $\Lambda = 4\,\mu$m, $q = 0.5$, and $h = 30$ nm on a GaAs. (*b*) Simulated (closed circles), theoretical (solid curve) and measured (cross point) of $n \cdot k$ as a function of area fill factor, q^2, for the metallic NiCr plates structure depicted in the upper right inset at 11 μm wavelength. Dashed curve represents effective medium approximation for a structure composed of metallic NiCr spheres. Open circles represent numerical calculation of a NiCr structure (0.1 μm period with 30 nm thickness). (*c*) Calculated absorption of a resonator configuration as a function of incident wavelength (at normal incident angle) for: NiCr subwavelength structure depicted in part (*a*) (solid curve); and 30 nm (dashed curve) of uniform NiCr thin film.

can be achieved by locally changing the metallic grating structure. It is also possible to exploit the proposed concept to manipulate the thermal emission for obtaining omnidirectional and broadband spectral thermal sources.

Acknowledgment

This research was supported by the Israel Science Foundation.

Nomenclature

c = speed of light in vacuum
λ = wavelength
ω = angular frequency
k = wavenumber
ε' = real part of dielectric constant
Λ = periodicity
q = filling factor
h = grating depth
Q = quality factor
ε = spectral emissivity
$\delta\omega$ = plasmonic bandgap width
R = harmonic amplitude ratio
ϕ = local orientation angle
Ω = rate of spatial rotation
θ = polar emission angle
σ = spin state
S_3 = Stokes parameter of circular polarization

References

[1] Greffet, J.-J., Carminati, R., Joulain, K., Mulet, J.-P., Mainguy, S., and Chen,Y., 2002, "Coherent Emission of Light by Thermal Sources," Nature (London), **416**, pp. 61–64.
[2] Marquier, F., Joulain, K., Mulet, J.-P., Carminati, R., Greffet, J.-J., and Chen, Y., 2004, "Coherent Spontaneous Emission of Light by Thermal Sources," Phys. Rev. B, **69**, p. 155412.
[3] Hesketh P. J., Zemel J. N., and Gebhart, B., 1986, "Organ Pipe Radiant Modes of Periodic Micromachined Silicon Surfaces," Nature (London), **324**, pp. 549–551.
[4] Wolf, E., 1987, "Noncosmological Redshifts of Spectral Lines," Nature (London), **326**, pp. 363–365.
[5] Dahan, N., Niv, A., Biener, G., Kleiner, V., and Hasman, E., 2005, "Space-Variant Polarization Manipulation of a Thermal Emission by a SiO_2 Subwavelength Grating Supporting Surface Phonon-Polaritons," Appl. Phys. Lett. **86**, p. 191102.
[6] Dahan, N., Niv, A., Biener, G., Kleiner, V., and Hasman, E., 2005, "Thermal Image Encryption Obtained With a SiO_2 Space-Variant Subwavelength Grating Supporting Surface Phonon-Polaritons," Opt. Lett., **30**, pp. 3195–3197.
[7] Hasman, E., Biener, G., Niv, A., and Kleiner, V., 2005 "Space-Variant Polarization Manipulation," *Progress in Optics*, Vol. 47, E. Wolf, ed., Elsevier, Amsterdam, p. 215.
[8] Niv, A., Biener, G., Kleiner, V., and Hasman, E., 2006, "Manipulation of the Pancharatnam Phase in Vectorial Vortices," Opt. Express, **14**, pp. 4208–4220.
[9] Pendry, J. B., 1999, "Radiative Exchange of Heat Between Nanostructures," J. Phys.: Condens. Matter, **11**, pp. 6621–6635.
[10] Wilde, Y. De, Formanek, F., Carminati, R., Gralak, B., Lemoine, P.-A., Joulain, K., Mulet, J.-P., Chen, Y., and Greffet, J.-J., 2006, "Thermal Radiation Scanning Tunnelling Microscopy," Nature (London) **444**, pp. 740–743.
[11] Kittel, A., Müller-Hirsch, W., Parisi, J., Biehs, S.-A., Reddig, D., and Holthaus, M., 2005, "Near-Field Heat Transfer in a Scanning Thermal Microscope," Phys. Rev. Lett., **95**, p. 224301.
[12] Rytov, S. M., Kravtsov, Y. A., and Tatarskii, V. I., 1989, *Principles of Statistical Radiophysics*, Springer-Verlag, Berlin.
[13] Shchegrov, A. V., Joulain, K., Carminati, R., and Greffet, J.-J., 2000, "Near-Field Spectral Effects due to Electromagnetic Surface Excitations," Phys. Rev. Lett., **85**, pp. 1548–1551.
[14] Carminati, R., and Greffet, J.-J., 1999, "Near-Field Effects in Spatial Coherence of Thermal Sources," Phys. Rev. Lett., **82**, pp. 1660–1663.
[15] Setälä, T., Kaivola, M., and Friberg, A. T., 2002, "Degree of Polarization in Near Fields of Thermal Sources: Effects of Surface Waves," Phys. Rev. Lett., **88**, p. 123902.
[16] Dahan, N., Niv, A., Biener, G., Gorodetski, Y., Kleiner, V., and Hasman, E., 2007, "Enhanced Coherency of Thermal Emission: Beyond the Limitation Imposed by Delocalized Surface Waves," Phys. Rev. B, **76**, p. 045427.
[17] Dahan, N., Niv, A., Biener, G., Gorodetski, Y., Kleiner, V., and Hasman, E., 2008, "Extraordinary Coherent Thermal Emission From SiC Due to Coupled Resonant Cavities," J. Heat Transfer, **130**, p. 112401.
[18] Ikeda, K., Miyazaki, H. T., Kasaya, T., Yamamoto, K., Inoue, Y., Fujimura, K., Kanakugi, T., Okada, M., Hatade, K., and Kitagawa, S., 2008, "Controlled Thermal Emission of Polarized Infrared Waves From Arrayed Plasmon Nanocavities," Appl. Phys. Lett., **92**, p. 021117.
[19] Lee, B. J., Fu, C. J., and Zhang, Z. M., 2005, "Coherent Thermal Emission From One-Dimensional Photonic Crystals," Appl. Phys. Lett., **87**, p. 071904.
[20] Lee, B. J., and Zhang, Z. M., 2007, "Coherent Thermal Emission From Modified Periodic Multilayer Structures," J. Heat Transfer, **129**, pp.17–26.
[21] Barnes, W. L., Preist, T. W., Kitson, S. C., and Sambles, J. R., 1996, "Physical Origin of Photonic Energy Gaps in the Propagation of Surface Plasmons on Gratings," Phys. Rev. B, **54**, pp. 6227–6244.
[22] Van Hove, L., 1953, "The Occurrence of Singularities in the Elastic Frequency Distribution of a Crystal," Phys. Rev., **89**, pp. 1189–1193.
[23] Pipino, A. C. R., Van Duyne, R. P., and Schatz, G. C., 1996, "Surface-Enhanced Second-Harmonic Diffraction: Experimental Investigation of Selective Enhancement," Phys. Rev. B, **53**, pp. 4162–4169.
[24] Kocabas, A., Ertas, G., Seckin Senlik, S., and Aydinli, A., 2008, "Plasmonic Band Gap Structures for Surface-Enhanced Raman Scattering," Opt. Express, **16**, pp. 12469–12477.
[25] Kitson, S. C., Barnes, W. L., and Sambles, J. R., 1995, "Surface-Plasmon Energy Gaps and Photoluminescence," Phys. Rev. B, **52**, pp. 11441–11445.
[26] Wang, Y., and Zhou, Z., 2006, "Strong Enhancement of Erbium Ion Emission by a Metallic Double Grating," Appl. Phys. Lett., **89**, p. 253122.
[27] Weeber, J.-C., Bouhelier, A., Colas des Francs, G., Markey, L., and Dereux, A., 2007, "Submicrometer In-Plane Integrated Surface Plasmon Cavities," Nano Lett., **7**, pp. 1352–1359.
[28] Descrovi, E., Paeder, V., Vaccaro, L., and Herzig, H.-P., 2005, "A Virtual Optical Probe Based on Localized Surface Plasmon Polaritons," Opt. Express, **13**, pp. 7017–1727.
[29] Biener, G., Dahan, N., Niv, A., Kleiner, V., and Hasman, E., 2008, "Highly Coherent Thermal Emission Obtained by Plasmonic Bandgap Structures," Appl. Phys. Lett., **92**, p. 081913.
[30] Balin, I., Dahan, N., Kleiner, V., and Hasman, E., 2010, "Bandgap Sructure of Thermally Exited Surface Phonon Polaritons," Appl. Phys. Lett., **96**, p. 071911.
[31] Balin, I., Dahan, N., Kleiner, V., and Hasman, E., 2009, "Slow Surface Phonon Polaritons for Sensing in the Midinfrared Spectrum," Appl. Phys. Lett., **94**, p. 111112.
[32] Garetz, B. A., 1981, "Angular Doppler Effect," J. Opt. Soc. Am., **71**, pp. 609–611.
[33] Lipson, S. G., 1990, "Berry's Phase in Optical Interferometry: A Simple Derivation," Opt. Lett., **15**, pp. 154–155.
[34] Bliokh, K. Y., 2009, "Geometrodynamics of Polarized Light: Berry Phase and Spin Hall Effect in a Gradient-Index Medium," J. Opt. A, **11**, p. 094009.

[35] Hosten, O., and Kwiat, P., 2008, "Observation of the Spin Hall Effect of Light via Weak Measurements," Science, **319**, pp. 787–790.
[36] Bliokh, K. Y., Niv, A., Kleiner, V., and Hasman, E., 2008, "Geometrodynamics of Spinning Light," Nat. Photon., **2**, pp. 748–753.
[37] Dooghin, A. V., Kundikova, N. D., Liberman, V. S., and Zel'dovich B. Y., 1992, "Optical Magnus Effect," Phys. Rev. A, **45**, pp. 8204–8208.
[38] Bliokh, K. Y., Gorodetski, Y., Kleiner, V., and Hasman, E., 2008, "Coriolis Effect in Optics: Unified Geometric Phase and Spin-Hall Effect," Phys. Rev. Lett., **101**, p. 030404.
[39] Gorodetski, Y., Niv, A., Kleiner, V., and Hasman, E., 2008, "Observation of the Spin-Based Plasmonic Effect in Nanoscale Structures," Phys. Rev. Lett. **101**, p. 043903.
[40] Dahan, N., Gorodetski, K., Frischwasser, Y., Kleiner V., and Hasman E., 2010, "Geometric Doppler Effect: Spin-Split Dispersion of Thermal Radiation," Phys. Rev. Lett., **105**, p. 136402.
[41] Gorodetski, Y., Nechayev, S., Kleiner, V., and Hasman, E., 2010, "Plasmonic Aharonov-Bohm Effect: Optical Spin as the Magnetic Flux Parameter," Phys. Rev. B, **82**, p. 125433.
[42] Gorodetski, Y., Shitrit, N., Bretner, I., Kleiner, V., and Hasman, E., 2009, "Observation of Optical Spin Symmetry Breaking in Nanoapertures," Nano Lett., **9**, pp. 3016–3019.
[43] Mauskopf, P. D., Bock, J. J., Del Castillo, H., Holzapfel, W. L., and Lange, A. E., 1997, "Composite Infrared Bolometers With Si_3N_4 Micromesh Absorbers," Appl. Opt. **36**, pp. 765–771.
[44] Becker, W., Fettig, R., and Ruppel, W., 1999, "Optical and Electrical Properties of Black Gold Layers in the Far Infrared," Infrared Phys. Technol., **40**, pp. 431–445.
[45] Niklasson, G. A., 1987, "Optical Properties of Gas-Evaporated Metal Particles: Effects of a Fractal Structure," J. Appl. Phys., **62**, pp. 258–265.
[46] O'Neill, P., and Ignatiev, A., 1978, "Influence of Microstructure on the Optical Properties of Particulate Materials: Gold Black," Phys. Rev. B, **18**, pp. 6540–6548.
[47] Cathelinaud, M., Lemarquis, F., and Amra, C., 2002, "Index Determination of Opaque and Semitransparent Metallic Films: Application to Light Absorbers," Appl. Opt., **41**, pp. 2546–2554.
[48] Bosman, H., Lau, Y. Y., and Gilgenbach, R. M., 2003, "Microwave Absorption on a Thin Film," Appl. Phys. Lett., **82**, pp. 1353–1355.
[49] Biener, G., Niv, A., Kleiner, V., and Hasman, E., 2007, "Metallic Subwavelength Structures for a Broadband Infrared Absorption Control," Opt. Lett., **32**, pp. 994–996.
[50] Cohen, R. W., Cody, G. D., Coutts, M. D., and Abeles, B., 1973, "Optical Properties of Granular Silver and Gold Films," Phys. Rev. B, **8**, pp. 3689–3701.